Long-Range AC Electroosmotic Trapping and Detection of Bioparticles

Jie Wu,[†,§] Yuxing Ben,[†,⊥] David Battigelli,[‡] and Hsueh-Chia Chang*[,†]

Center for Micro-fluidics and Medical Diagnostics, Department of Chemical and Biomolecular Engineering, University of Notre Dame, Notre Dame, Indiana 46556, Scientific Methods, Inc., Granger, Indiana 46530, Department of Electrical and Computer Engineering, The University of Tennessee, Knoxville, Tennessee 37996, and Department of Mathematics, Massachusetts Institute of Technology, Cambridge, Massachusetts 02139

Microfluidic devices with integrated electrical detection will enable fast, low-cost or portable sensing and processing of biological and chemical samples. By employing microfabrication, micro-electrical impedance spectroscopy detectors are designed to take advantage of AC electroosmosis to rapidly concentrate bioparticles, leading to enhanced sensitivity due to a reduction of the transport time to the detector. Electrodes were fabricated by integrated circuit technology. Experiments were performed to find the optimal voltage and frequency ranges such that a trapping converging flow exists on the electrodes and the assembled cells exhibit sensitive impedance spectrum signatures. Preliminary results show resolution at a concentration of 10^4 bacteria/mL, indicating that combining AC electroosmosis with impedance measurement can improve the sensitivity and speed of detection of bacteria in solutions with conductivity comparable to that in environmental applications. The bacterial impedance signatures are, however, different in tap water and PBS buffers, due perhaps to different ion transport properties across the cell membranes in the two solutions.

Introduction

Recent years have witnessed many developments in microfluidic and micro total analysis systems (μTAS) by applying microfabrication techniques to biological and chemical analysis. Integrating microscale detectors with fluid transport systems on one chip has significant advantages, including increased resolution, faster response, smaller sample sizes, and increased parallelism of analysis.

Detection of microorganisms such as bacteria and viruses is important in a variety of fields, such as bioscience research, medical diagnosis, screening analysis in food processing and for environmental testing. However, miniature medical and environmental diagnostic kits that are portable and fast have yet to be developed. One reason is that biosensors function effectively as detectors only when the bacteria or viruses are proximal and only when sufficient particles are present to stimulate signal generation. For practical applications, biosensors must offer a sensitivity that can detect fewer than 1000 microorganisms per milliliter of suspension. Conventional microbiological detection methods rely upon enrichment techniques in which bacteria are incubated on nutrient media or viruses are incubated on cell cultures. The time required for cultures to produce unambiguous indications of growth may range from days to several weeks, rendering these methods cumbersome and occasionally impractical for point-of-care diagnosis or emergencies.

There are mainly two groups of particle detection schemes in the absence of culture or enzymatic amplification (e.g., PCR). One is optical detection, which is commonly realized through UV detectors, fluorescence detectors, and refractive index detectors. For large-scale laboratories with sophisticated equipment and trained personnel, these detection techniques provide adequate sensitivity and rapid results. However, these techniques are not well-suited for integration with microsystems. Another group of detection strategies uses electrical characterization, which scans the detection volume with an electrical frequency sweep over a range of frequencies. One method is electrical impedance spectroscopy (EIS), inspecting both real and imaginary parts of impedances typically from tens of hertz to megahertz. EIS systems are simpler to construct than optical systems and more compatible with microtechnology, as well as more reliable.[1] There have been reports on microfabricated EIS prototypes intended for microfluidic systems, which are based on changes in solution conductivity.[2−4]

Here, we report an EIS scheme that utilizes AC electrokinetics to concentrate particles[5] for enhanced selectivity. Particles suspended in fluid could experience forces when subjected to AC electric fields, which could be a dielectrophoretic force due to field-induced particle polarization or a viscous drag force due to electroosmotic flow generated by double layer polarization on channel walls or on electrodes. Due to the small dimensions of microfabricated electrodes, a relatively intense electric field for significant dielectrophoresis (DEP) or electroosmosis (EO) can be obtained with relatively low voltages applied over the electrodes. We use electroosmotic flow, generated by field-induced electrode polarization, to convect particles from the bulk of the suspension to the electrode surface, where the presence of particles has a larger impact on impedance measurements than in the bulk.

It has been well-documented that DEP can be used for the manipulation and characterization of particles

* To whom correspondence should be addressed. Tel.: (574) 631-5697. Fax: (574) 631-8366. E-mail: chang.2@nd.edu.

[†] University of Notre Dame.

[‡] Scientific Methods, Inc..

[§] The University of Tennessee.

[⊥] Massachusetts Institute of Technology.

10.1021/ie049417u CCC: $30.25
Published on Web 02/15/2005

and the separation of mixtures, such as cells, bacteria, and latex spheres.[6–9] Suehiro et al.[10] have demonstrated a combination of DEP with electrical rupture of cell structure to increase detection sensitivity. However, DEP is particle-size-sensitive and of rather short range; therefore, it is not effective for manipulating micrometer and submicrometer bioparticles, such as bacteria and viruses more than 20 μm away from the electrodes. It also relies on field gradient and, hence, usually requires small interdigitated electrodes. Such electrodes with narrow electrodes also have short field penetration lengths and, hence, are ineffective for bacteria that are more than one electrode width of about 20 μm away.

On the other hand, electroosmotic motion has no dependence on particle size and scales much more favorably with the distance from the electrode ($1/r$ versus $1/r^3$ for DEP). It can also be driven by wide electrodes whose EO flow fields can span several millimeters or centimeters. Therefore, the viscous drag force by such long-range and intense EO flow is particularly advantageous for collecting micrometer/submicrometer particles from the electrolyte. Green et al.[11] have investigated in detail microfluidic flows on the surface of a coplanar electrode pair and documented AC EO flow rates as a function of electrolyte conductivity, signal frequency and potential, and position on the electrode surface. Their characterization sheds much light on a particular AC EO mechanism by "capacitive charging". Wong et al.[12] and Hoettges et al.[13] have reported the aggregation of particles on electrode surfaces, which they attributed to a combination of dielectrophoretic and electrohydrodynamic forces. In this paper, we further explore and delineate the various ACEO mechanisms, including a new Faradaic charging mechanism at high voltages. We find that trapping only occurs within a particular voltage and frequency window when a converging stagnation flow exists. We also investigate the importance and design of a local particle force field at the stagnation line. The properly optimized AC EO flow allows extremely rapid concentration of bacteria from a dilute suspension to a localized sensor position such that the sensor's speed and sensitivity can be enhanced significantly. In fact, we utilize the same electrodes that induce AC EO as impedance sensors in the current design by properly selecting the AC frequencies to capture the existence of the bacterial assembly.

Since AC scanning signals are adopted in EIS detection, AC electrokinetics can be readily combined with EIS. A properly designed device could even induce the necessary AC EO with the same frequency scan for EIS detection. Measuring cell impedance at an AC potential appropriate for inducing surface flow and particle assembly, we have observed an increased differentiation of impedances between bacteria suspensions and buffer solutions within certain frequency and voltage windows. These windows produce the proper trapping AC EO flow as well as enhanced EIS sensitivity for detecting the assembled bacteria. However, the bacterial signatures are different in tap water and PBS buffers. Within 1 min, we are able to induce bacterial self-assembly along the stagnation line of each electrode. The bacterial lines represent an increase in concentration by 4 orders of magnitude relative to the bulk. Using just one pair of pumping/sensor electrodes, the sensitivity of our detector can reach 10^4 bacteria/mL.

AC Electroosmotic (EO) Flow. Electroosmosis depends on surface charges at the electrode/electrolyte interface. Most materials will acquire fixed surface charges when coming into contact with a fluid that contains ions (either an electrolyte or a dielectric liquid with ionic impurities or generated locally via reactions). The surface charges attract counterions from the solution and repel co-ions from the surface to maintain local charge neutrality. Consequently, an excess of charges is built up near the electrode surface, thus forming an electrical double layer. The ions in the electrical double layer are mobile and will migrate under the influence of an electric field tangential to the electrode surface. Due to fluid viscosity, fluid surrounding the ions will move along, inducing so-called electroosmosis. The slip velocity at the outer plane of the double layer is $u_t = -(\epsilon/\mu)\zeta E_t$, where E_t is the tangential electric field; μ is the viscosity of the fluid; and ζ is the potential drop across the double layer, which is an indication of charge density in the doubly layer.

This phenomenon has been applied to build DC electroosmotic pumps,[14] in which the electric field tangential to the double layer is imposed by two electrodes at the ends of microchannels. To achieve sufficient electric field strengths over the length of microchannels, DC pumps have to use high voltages and consequently suffer from electrolysis at the electrodes, which produces bubbles. Open reservoirs are almost indispensable with DC EO devices because generated gas has to be vented, which could introduce uncontrolled pressure differences, sample contamination, etc. High potentials also cause electrochemical reactions and lead to pH gradients.[15] Additionally, because electric field lines have the same contour as streamlines, it is hard to realize effective mixing with DC pumps.

To circumvent those problems, there is considerable recent interest in AC EO, which suppresses undesirable reactions by energizing embedded microelectrodes with high-frequency potentials. If the frequency is larger than or comparable to the inverse reaction time at the given voltage, net electrolysis and other Faradaic reaction products can be avoided, and the electrodes can be embedded within the channels. Similar to DC EO, AC EO is also generated by exerting a force on double layer charges at solid/liquid surface by tangential electric fields. The electrical potentials over electrodes induce net charges in the electrical double layer and in the meantime provide tangential electric fields to drive the ions. Because charges in the double layer and electric fields change directions simultaneously, AC EO produces steady local vortices above the electrodes, as shown in Figure 1. These vortices are driven by opposite (outward) time-averaged slip velocities on the two electrodes due to the AC charging mechanisms on their double layers.

Our earlier analysis[16] of the surface E-fields for symmetric electrode charging reveals that, for very wide electrodes, the tangential electric fields switch directions at $1/\sqrt{2}$ of electrode width away from its inner edge, as shown in Figure 2a. Because flow directions depend on the tangential fields, four counter-rotating vortices were formed at the electrode surface, and the stagnation takes place at locations where tangential fields become zero, as shown in Figure 2b.

There exist several electrode processes when an electric potential is applied over the electrodes in an electrolyte. Electric potentials from the electrodes can

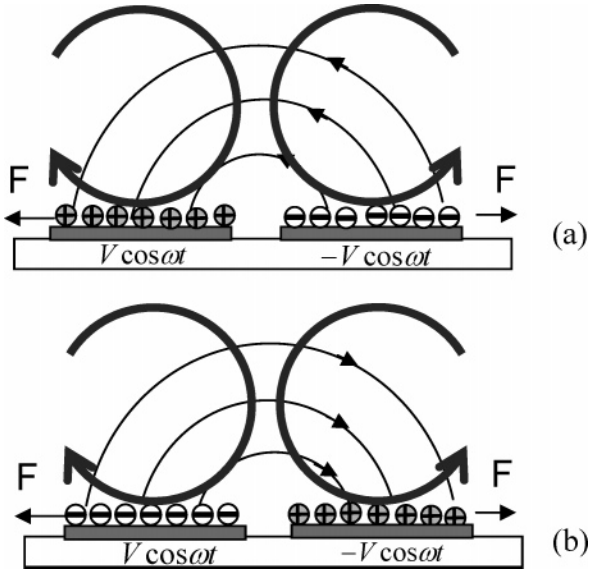

Figure 1. AC electroosmosis by capacitive charging of a planar electrode pair. Flow motion and induced charges at electrode surface (a) during the half cycle when the left electrode has a negative polarity, and (b) during the next half cycle with opposite electrical polarity.

attract counterions from the electrolyte to screen the electrode potential (aka *capacitive charging*) or *generate* co-ions from electrochemical reactions at the electrodes following Faraday's law (aka *Faradaic charging*) when the electrode is positively charged. Electrode polarization by capacitive charging has been widely recognized and has been used to generate AC EO,[17] whereas the polarization by Faradaic charging and related EO are reported only recently by our group.[16,18−20]

Capacitive and Faradaic charging produce ions of opposite signs in an electrical field, which in turn result in EO flows in opposite directions. However, capacitive charging cannot produce a polarization exceeding the equilibrium charge density on the electrode side, whereas Faradaic charging can produce charge densities orders of magnitude beyond equilibrium values. In addition, the two polarizations have different dependence on the applied voltage, and so are the slip velocities, u_t, induced by two polarizations. For capacitive charging, $u_t \sim V^2$, whereas for Faradaic charging, $u_t \sim \exp(V)$. We have exploited this larger slip velocity by Faradaic charging to design micropumps and micromixers by using asymmetric electrode geometry to produce a net flow.[20] However, for bioparticle concentration and detection, the classical parallel electrode design with two symmetric vortex pairs remains optimal.

Nevertheless, even for parallel electrodes, the AC EO flow fields and their bioparticle trapping efficiencies due to capacitive and Faradaic charging are quite distinct and must be designed with care. Because there is a threshold voltage for Faradaic reaction to occur at a given frequency, capacitive charging predominates at low voltages, whereas Faradaic charging takes over at higher voltages with its exponential dependence on potential. In addition, capacitive and Faradaic charging possesses different dependence on frequency. Faradaic charging becomes stronger at lower frequency, while capacitive charging has an optimal frequency depending on electrode geometry and electrolyte conductivity. Hence, the operating frequency cannot be excessively low if capacitive charging is desired. Generally speaking, AC EO due to capacitive charging vanishes for high-conductivity buffers[11] but not AC EO due to Faradaic charging. These high-conductivity fluids have very thin double layers (<10 nm) and double layer polarization by capacitive charging can only be achieved at frequencies too high for most power supplies, whose signals at such frequencies are corrupted by parasitic RC times of the entire system circuit.

At the stagnation point, capacitive charging produces converging surface flows and Faradaic charging produces diverging ones—the field lines are nearly identical but with opposite directions. Particles on the surface are swept toward converging stagnation lines and away from diverging ones. However, if the only force on the particles is viscous drag exerted by the electroosmotic vortex, the particles would be resuspended from the stagnation line and would not be trapped. The particle trajectory would be identical to the streamline in this case, and the solenoidal nature of incompressible flow renders the stagnation point a saddle point rather than a sink. Hence, a local nonhydrodynamic force field must be applied on the particle at the stagnation point, where the electroosmotic flow and electrode slip velocity and their corresponding viscous drags are weakest. For a converging stagnation point, a normal particle force toward the electrode would be sufficient to trap the particles, but for a diverging stagnation line, a trapping force field radially directed toward the stagnation line must be imposed. The sink of the latter local field must be aligned with the diverging stagnation line. In contrast, the local field for a converging stagnation line need not have a sink—it can be unidirectional or even uniform. It is, hence, much easier to trap particles at a converging stagnation line. The corresponding local particle force field can be the gravitational field for nonneutrally buoyant particles or a magnetic field for magnetic particles or bacteria anchored to magnetic beads. Because the electric field on the electrode surface is higher than further above, a particle suffering positive DEP can also be trapped at the stagnation line. Hence, by choosing the appropriate charging mechanism and the appropriate local particle field, particles can be trapped and concentrated on the electrodes. Subsequently, electrodes with particle assembly lines are ready for impedance measurements to achieve high-sensitivity particle detection. A better alternative strategy to be attempted is to carry out the assembly and detection in parallel.

Electrical Impedance Spectroscopy. The dynamic impedance between the electrodes, when an AC voltage or current is imposed, is determined by dielectric and conducting properties of the electrodes and the electrolyte, as well as chemical interactions between the metal and the ions in the electrolyte. Impedance spectroscopy can, hence, be used to differentiate the capacitive and Faradaic charging mechanisms without flow field visualizaton. Bacteria accumulation on the electrode is expected to disrupt some of these dynamic current−voltage correlations. To identify the relative impacts of the various charging and ion transport mechanisms at different frequencies and voltages, an electrical equivalent circuit is developed for the electrode pairs under test, as shown in Figure 3.

In Figure 3, R_{lead} represents lead resistance, which arises from the thin film metal lines, bonding pads, etc.; therefore, they are in series with the electrolytic cell. C_{cell} accounts for direct capacitive coupling between the two electrodes. The value of C_{cell} depends on the

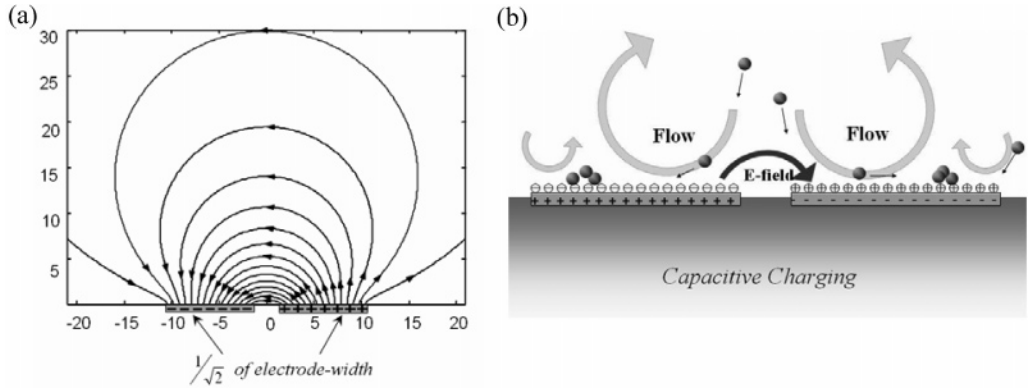

Figure 2. Electric field distribution and induced flow motion above a pair of capacitively charged electrodes in an electrolyte. (a) Electric field distribution above a pair of planar electrodes. The tangential component changes sign at the predicted stagnation lines (axes: relative dimensions). (b) With capacitive charging, four counter-rotating vortices are formed above the electrodes due to changes in tangential electric fields. At an appropriate strength of electrode polarization, particles aggregate at the stagnation points.

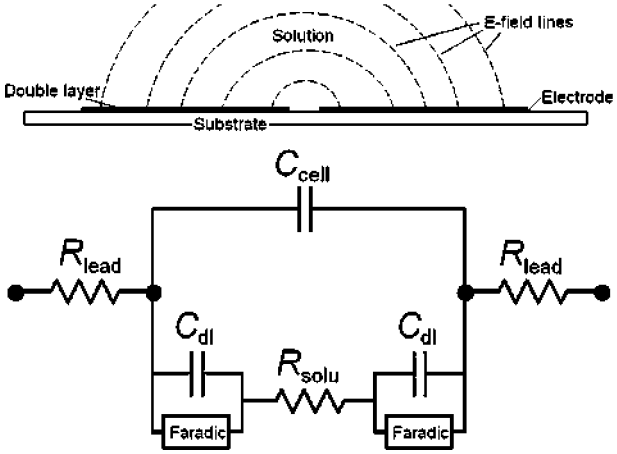

Figure 3. Equivalent circuit for the planar parallel detection electrodes.

dielectric properties of the electrolyte and electrode geometries. The bulk of the electrolyte obeys Ohm's law, so the bulk of the solution is modeled as a resistor, R_{solu}, in series with components at the interfaces of the electrodes and the electrolyte.

There are several current conducting and charge accumulation mechanisms at the electrode−electrolyte interface. Hydrolyzed ions at the surface of metal electrodes cause a double layer capacitance, C_{dl}. There are also electrode reactions at the interface, which is represented by a Faradic impedance in our equivalent circuit. If there is an electrode reaction, electric charges are transferred across the interface in parallel to the charging of the double layer, so the Faradic impedances are in parallel with C_{dl}. Faradic impedances are typically modeled as a battery (for the DC half-cell potential), an electron-transfer resistor, and a Warburg impedance (for ion diffusion) in series.

The relative importance of circuit components determines frequency response of the electrode impedance. Because of the small thickness of double layers, C_{dl} is generally much larger than C_{cell}. Therefore, at low frequencies, voltage drops mostly happen at the electrode−electrolyte interface, and the cell impedance behaves somewhat like a capacitor. However, due to electrode reactions, there is a resistive component, so the Bode modulus plot deviates from a −20 dB/decade (or −decade/decade) downward slope in a log−log plot. Since it is difficult to discern Faradaic reaction at the electrode from charge transfer from the assembled bacteria, we shall select frequencies and voltages at which Faradaic reactions do not occur at the electrode and the low-frequency spectra exhibit the characteristic −20 dB/decade line of a capacitor.

As the frequency increases, the admittance across the double layer becomes smaller, and more current flows through the resistive bulk of the solution, so the impedance spectrum approaches a flat line, and that is the bulk resistance, R_{solu}. At higher frequencies, the dielectric coupling of the electrodes dominates the cell impedance, and the impedance curve becomes a −20 dB/decade line again. Since the cell impedance is sensitive to electrode and sample dimension and since the assembled bacteria are at the electrode surface and not in the bulk, it is not desirable to use the high-frequency spectra for bacteria detection.

It can be deduced that at low to medium frequency, the electrode double layer impedance dominates the current conducting path due to counterion charging, and most of the applied voltage drops over the electrical double layer. It is, hence, the frequency range where the impedance difference from particle assembly is detectable. There is yet another important reason to use low frequencies.

The equivalent circuit of Figure 3 fails to capture the distributed nature of the electric field over the finite-width electrode pair. The field strength at the stagnation line in Figure 2, where the bacteria are assembled, can, hence, change with electrode geometry. The contribution of the assembled bacteria to the electrode capacitance would also be geometry-dependent. To produce a robust detection scheme, we shall examine only the low-frequency limits of the impedance spectrum. At this low-frequency limit, the voltage drop is mostly across the double layer and not the bulk. There is, hence, little dependence on the bulk dimension, that is, the gap separation. The concentrated low-frequency field at the electrode surface should also be uniform across the electrode, thus removing the electrode width dependence. (The complex impedance is the ratio of the Fourier amplitude of the total voltage drop over the corresponding total current. With a uniform current and voltage across the electrode, the width dependence also vanishes.) As such, the spectra at low frequency should be weakly dependent on the electrode gap separation, the electrode width, or any electrode dimension. A key to this electrode insensitivity is the invariance of the −20 dB/decade line to electrode geometry. For the same electrolyte, this asymptote should be geometry-inde-

pendent. In contrast, the high-frequency −20 dB/decade asymptote would be geometry-dependent because the field penetration depth into the bulk in this limit is specified by the electrode gap separation and width.

When the electrodes are charged by co-ions due to Faradaic charging and not counterions due to capacitive charging, the field is no longer confined to the double layer, and in fact, the bulk field is intensified by co-ion charging. As a result, geometry dependence occurs for Faradaic charging. Hence, the rms voltage drop should be high enough to effect the capacitive charging of the double layer but not too excessive to trigger Faradaic reaction. By the same token, the frequency should be sufficiently low to probe the electrode surface but not too low such that Faradaic reactions occur. These voltage and frequency considerations are also important for the assembly process, because only the converging flow of capacitive charging can trap bacteria. We shall demonstrate the design considerations to achieve these conditions in the next section.

Experiments

The detection of particles was carried out with a pair of Ti/Au (10 nm/90 nm) parallel microelecrodes. Ti is the adhesion layer between the substrate and Au, and Au is in contact with electrolytes. Planar microfabrication techniques were used to fabricate electrodes on glass substrates. The procedure is as follows: Depositing a layer of SiN_x on glass substrates to promote photoresist adhesion, applying photoresists and patterning electrodes for metal lift-off, electron-beam evaporating 0.1 μm thick metals, and immersing samples in acetone to obtain electrodes.

The electrodes were 20 mm long and 0.1 μm thick. However, a range of gap separations and electrode widths were used. The most common two geometries were 80-μm width and 40-μm gap and 40-μm width and 20-μm gap. R_{lead} was calculated to be ~18 Ω for Ti/Au electrodes. Because the cell impedance is determined to be over several kiloohms, the electric field distribution in the electrodes lengthwise is expected to be uniform.

A. Particle Collection. The first set of experiments was to determine appropriate potentials and frequencies for bioparticles to assemble at the stagnation positions indicated in Figure 2. The electrode chambers were formed by sealing silicone microchambers (PC8R-0.5, Grace Bio-Labs, Inc.) over the glass slides, so electrode pairs of ~9 mm length were exposed to electrolytes; the electrode chambers had a height of 500 μm.

First, polystyrene spheres at a diameter of 5 μm (Fluka Chemica 79633) were used at a particle concentration of ~5.0×10^6 particles/mL. Particles were suspended in deionized (DI) water. An HP33120 signal generator was used to apply electrical potential to the electrodes. A frequency range from 20 Hz to 1 kHz was determined to be optimal for observing particle motion in the DI water suspension, and 100 Hz was used in the following particle assembly experiments.

Figure 4 shows four frames of particle motion on the electrode surface. The frames were taken at 0, 5, 10, and 15 s after the field was turned on. The initial voltage was 1.0 Vrms and was increased to 2.2 Vrms at 10 s. Particles on the electrodes in the first two frames, a and b, are seen to move in directions consistent with electroosmotic flow due to capacitive charging and assemble into lines. Particles convected by the capacitive flow would need to move vertically upward in the planes

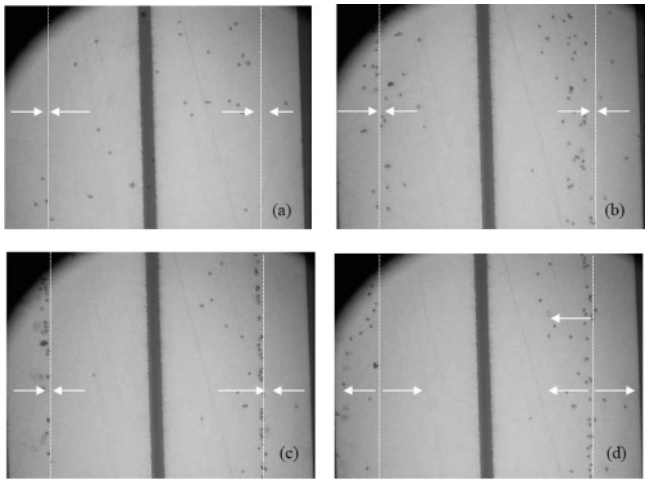

Figure 4. The assembly and erasure processes for Au electrodes at a frequency of 100 Hz. At $V = 1$ Vrms, the particle assembly takes place at the predicted stagnation line in frames (a) and (b) due to the converging stagnation flow of capacitive charging. At 2.2 Vrms, the particles are swept away from the stagnation line by the diverging stagnation flow of Faradaic charging in frames (c) and (d). The arrows indicate the directions of particle motion. The dashed lines are at the predicted stagnation line.

of stagnation line. However, the vertical flow is weak at the stagnation point, and an opposite vertical force such as gravity can prevent this vertical motion away from the electrodes. The particles would then be trapped at the stagnation lines, as seen in Figure 4. Sedimentation certainly plays a part in attaching particles to the electrode surface, since the stagnation lines are not observed when the electrodes are facing downward. Other possible local forces include the DEP force that attracts particle to high-field region. However, typical DEP phenomena such as assembly near electrode edges and levitation are not observed for a range of particle sizes from 1 to 5 μm, and even for high-conductivity buffers in which AC EO flow is weak, suggesting that DEP particle forces are not important in the current experiments because the electric field gradient is relatively weak due to the relatively large electrode geometries.

Faradaic flows at the stagnation locations are diverging and nontrapping with the unidirectional local force. Therefore, in the subsequent two frames, c and d, when the applied voltage is at 2.2 Vrms, particle lines are erased by Faradaic charging. To effectively convect particles to the electrode surface and deposit them there, it is important that there are converging flows toward the stagnation lines and that the flows are not too strong that the upward force outbalances the gravity, DEP, and other surface force.

Subsequently, *Escherichia coli* was used to test the applicability of the foregoing concept. Using 1 Vrms at 100 Hz, lines of bacteria were formed within 30 s on the electrode surface from a 4×10^6 CFU/mL suspension, as shown in Figure 5.

B. Impedance Measurement and Interpretation. After determining the optimal potential of 1.0 Vrms for trapping bioparticles at the electrode surface with converging flow due to capacitive charging, we proceed to measure the cell impedance at the appropriate potential. Here, we need to scan a range of frequencies, and we will find the frequency range at 1.0 Vrms that cannot sustain Faradaic reactions, unless the assembled bacteria are swept away, as in Figure 4.

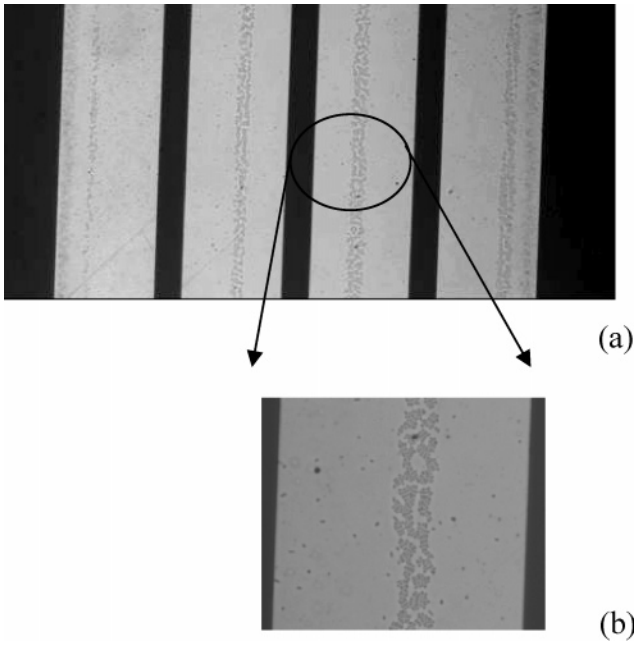

Figure 5. Assembled *E. coli* lines on an array of electrodes at 1 Vrms.

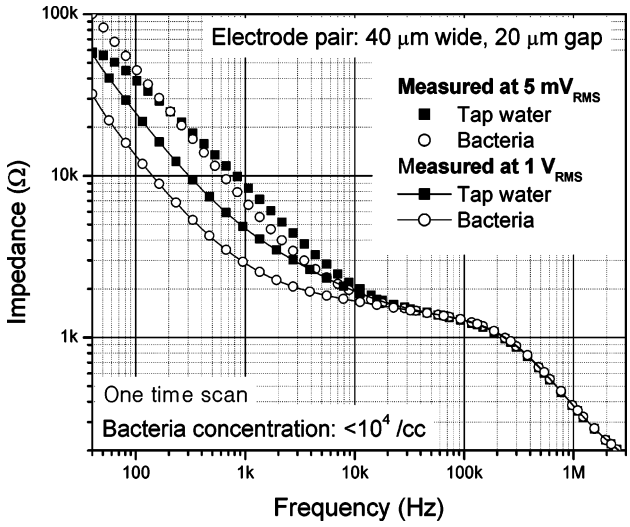

Figure 6. Impedance spectra of *E. coli* in tap water at 1 Vrms.

The electrode impedances were measured with an Agilent 4294A impedance analyzer from 40 Hz to 5 MHz at an open oscillation level of 5 mVrms and 1.0 Vrms. Appreciable AC EO is not expected at 5 mVrms, and this controlled experiment is to verity the effect of AC EO trapping at 1.0 Vrms. Although AC EO converging flow by capacitive charging is expected to be optimal at an intermediate frequency of ~1 kHz, scanning the entire range of frequency is not expected to disrupt the trapping process, provided sufficient time is allowed near the optimum frequency. In this manner, the trapping and sensing are achieved in one scan.

First, *E. coli* were resuspended in tap water of 2 mS/M at 5×10^3 CFU/mL. Measured impedance spectra are given in Figure 6. The modulus of the complex impedance is plotted for all impedance spectra. However, the low and high frequency spectra are mostly imaginary, representing inverse capacitance of the double layer and the medium, respectively, with the distinct −20 dB/decade line discussed in the equivalent circuit of Figure 3. For the measurements at 5 mV, little difference between *E. coli* suspensions and control tap water can be detected. As a comparison, the measurements of the same samples at 1 Vrms exhibit impedance difference by a factor of 2. The impedance difference appears at frequency lower than a few kHz, where the interfacial impedance dominates the whole cell impedance. The imaginary impedance is smaller when bacteria are assembled at the stagnation line, indicating increase in electrode capacitance when the bacteria are concentrated at the stagnation line. The bacterial assembly provides more surface area for charge accumulation and, hence, the increase in capacitance. Beyond 10 kHz, all of the impedance spectra at all voltages and with or without bacteria converge, indicating only the universal bulk dielectric response is detected.

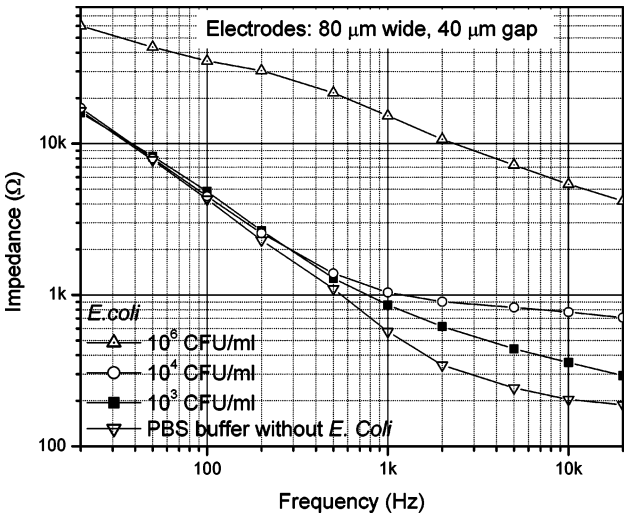

Figure 7. Impedance spectra of *E. coli* in PBS at 1 Vrms.

Another set of impedance measurements was performed on *E. coli* suspended in PBS buffer, which has a conductivity of 0.18 S/m. The measured spectra are shown in Figure 7. We note that when the bacteria are not detected, the all of the low-frequency impedance spectra of Figures 6 and 7 exhibit the universal −20 dB/decade slope, despite the fact that their electrode dimensions are different by a factor of 2. There is a slight shift between Figures 6 and 7, which can be attributed to the weak (square root) dependence of the capacitance on conductivity. Although one electrode is twice as large as the other, the shift is much weaker than this geometric scaling. This confirms the data at low frequency are insensitive to electrode dimensions. It is also evident in Figure 7 that at 1.0 Vrms and at frequencies above 40 Hz, there is no Faradaic reaction at the electrode for the PBS sample. As shown in the equivalent circuit of Figure 3, any Faradaic reaction would corrupt the −20 dB/decade asymptotic slope at low frequencies. Hence, at 1 Vrms and at above 40 Hz, there is no Faradaic reaction at the electrode, and the electrode double layer can be probed for the presence of assembled bacteria.

In contrast, the high-frequency data of Figures 6 and 7 are very different, indicating strong dependence on electrode geometry when the voltage drop is most across the bulk. The high-frequency spectra of the PBS sample in Figure 7 do not even exhibit the expected −20 dB/decade slope. The reason for this deviation from the expected high-frequency asymptote seen in the tap water spectra of Figure 6 will be explored below.

Compared with tap water suspensions, PBS suspensions with detectable bacteria presence exhibit impedance differences at low frequencies only beyond a threshold concentration, although the high-frequency spectra show bacteria sensitivity at all concentrations. Moreover, at both limits, the impedance increases as *E. coli* concentration increases, suggesting the capacitance charge storage effect is overwhelmed by a parallel charge transfer effect. We suspect the live bacteria are able to release and absorb cations through their ion pumps and ion channels in a buffer solution. At low frequencies, this co-ion charge transfer at the assembled bacteria line promotes ion transport and, hence, reduces the capacitance of the double layer, despite the increase in surface area. This corresponds to an increase in the low-frequency imaginary impedance, as seen in Figure 7. Moreover, unlike the tap water data of Figure 6, the imaginary impedance increases at high frequency with increasing bacteria concentration, even when the low-frequency data remain indistinguishable. Because the high-frequency spectra probe mainly the bulk buffer and at least some of the bacteria are believed to remain suspended in the bulk under these conditions, this trend again suggests that the *E. coli* are promoting ion transport in the bulk through their membranes, and the capacitance of the medium hence decreases. In contrast, the bacterial self-assembly on the electrodes can only be probed at low frequencies, and its effect shows up only beyond a critical concentration, albeit the sensitivity is much larger at low frequency beyond this threshold.

Although it is tempting to use the high-frequency spectra of the PBS solution to detect bacterial content in the bulk, we find it to be very sample-volume- and electrode-geometry-sensitive. The high-frequency spectra of Figure 7 are quite different from Figure 6, although the low-frequency data of both without bacterial signature are quantitatively indistinguishable. The low-frequency data with bacterial signature are quite distinct for the two solutions because of the different membrane ion transport properties of the bacteria in the two solutions. It is, hence, more robust to use the low-frequency data of both solutions between 40 Hz and 10 KHz with a bacterial detection threshold of 10^3 CFU/mL, which is roughly the literature benchmark for bacterial detection without culturing. By knowing the approximate frequency to use in the impedance spectroscopy, we may not need to scan a large frequency range and use one frequency for both the trapping and detection.

The fact that there exists a low-frequency bacterial detection threshold for the high-conductivity buffer solution in Figure 7 suggests that the converging AC EO flow becomes weaker for strong electrolytes. We expect and found in some preliminary experiments that, for a sufficiently high-conductivity medium, the AC EO flow that assembles the bacteria will eventually become too weak to concentrate the bacteria at any concentration. However, the current buffer conductivity and tap water already represent the most practical conductivity range for environmental bacterial detection.

Conclusions

This paper describes a method to improve the detection limits of bioparticles by electrical impedance spectroscopy. Particle and bacterial assembly by AC electroosmosis were demonstrated, and surface flow motion by different electrode polarization was investigated. Converging surface flow on the electrodes due to capacitive charging, which occurs within a particular voltage and frequency range, is found to be optimal for trapping bacteria at the electrodes. The proper voltage frequency and voltage range to ensure capacitive charging without Faradaic reactions is, indeed, found for a set of parallel electrode designs. The trapped bacteria produce a strong impedance signature at low frequencies that is insensitive to electrode geometry and sample volume, because screening by the double layer charges confines the field to the electrode surface and renders it nearly uniform. Incorporating particle assembly with impedance spectroscopy shows promise for enhanced sensitivity in particle detection at point-of-care diagnostic applications.

We are currently developing and optimizing a prototype kit for electroosmosis bioparticle trap based on these preliminary results. The objective is to use a single frequency for both trapping and detection such that the frequency scan does not have to be carried out. The sensitivity and detection time of the kit will be reported in a future publication.

Acknowledgment

Y.B. and H.C.C. are supported in part by a NASA grant.

Literature Cited

(1) Gale B. K.; Frazier A. B. Electrical impedance-spectroscopy particle detector for use in microanalysis systems. *SPIE Symp. Micromach. Microfab.: Micro Fluidic Dev. Syst.* Santa Clara, CA, September 20−21, 1999; pp 190−201.

(2) Ayliffe H. E.; Frazier A. B.; Rabbitt, R. D. Electric impedance spectroscopy using microchannels with integrated metal electrodes. *J. Microelectromech. Syst*. **1999**, *8*, 50−57.

(3) Ayliffe H. E.; Rabbitt R. D. An electric impedance based microelectromechanical system flow sensor for ionic solutions. *Meas. Sci. Technol.* **2003**, *14*, 1321−1327.

(4) Gomez, R.; Bashir, R.; Sarikay, A.; Ladisch, M. R.; Sturgis, J.; Robinson, J. P.; Geng, T.; Bhunia, A. K.; Apple, H. L.; Wereley, S. Microfluidic biochip for impedance spectroscopy of biological species. *Biomed. Microdev.* **2001**, *3*, 201−209.

(5) Wu, J.; Chang, H.-C. Long-Range Electrokinetic Bioparticle Trap. *AIChE annual meeting 2004*, Nov. 7−12, Austin, TX.

(6) Ramos, A.; Morgan, H.; Green, N. G.; Castellanos, A.; The role of electrodrodynamic forces in the dielectrophoretic manipulation and separation of particles. *J. Electrost.* **1999**, *47*, 71−81.

(7) Hughes, M. P.; Morgan, H. Dielectrophoretic characterization and separation of anibody-coated submicometer latex spheres. *Anal. Chem.* **1999**, *71*, 3441−3445.

(8) Morgan, H.; Hughes, M. P.; Green, N. G. Separation of submicron bioparticles by dielectrophoresis. *Biophys. J.* **1999**, *77*, 516−525.

(9) Auerswald, J.; Knapp, H. F. Quantitative assessment of dielectrophoresis as a micro fluidic retention and separation technique for beads and human blood erythrocytes. *Microelectron. Eng.* **2003**, *67−68*, 879−886.

(10) Suehiro, J.; Hamada, R.; Noutomi, D.; Shutou, M.; Hara, M. Selective detection of viable bacteria using dielectrophoretic impedance measurement method. *J. Electrost.* **2003**, *57*, 157−168.

(11) Green, N. G.; Ramos, A.; Gonzalez, A.; Morgan, H.; Castellanos, A. Fluid flow induced by nonuniform ac electric fields in electrolytes on microelectrodes. I. Experimental measurements. *Phys. Rev. E.* **2000**, *61*, 4011−4018.

(12) Wong, P. K.; Wang, T.-H.; Deval, J. H.; Ho, C.-M. Electrokinetics in Micro Devicesfor Biotechnology Applications. *IEEE/ASME Trans. Mechantronic* **2004**, *9*, 366−376.

(13) Hoettges, K. F.; McDonnell, M. B.; Hughes, M. P. Use of combined dielectrophoretic/electrohydrodynamic forces for biosensor enhancement. *J. Phys. D: Appl. Phys.* 36, **2003**, L101−L104.

(14) Chen, C.-H.; Santiago, J. G. A planar electroosmotic micropump. *J. Microelectromech. Syst.* **2002**, *11*, 672−683.

(15) Minerick, A. R.; Ostafin, A. E.; Chang, H.-C. Electrokinetic transport of red blood cells in micocapillaries. *Electrophoresis* **2002**, *23*, 2165−2173.

(16) Ben, Y.; Wu, J.; Chang, H.-C. Linear particle assembly and erasure by AC electro-osmotic Flow. Submitted to *Phys. Rev. E*.

(17) Ramos, A.; Morgan, H.; Green, N. G.; Castellanos, A. AC electrokinetics − a review of forces in microelectrode structures. *J. Phys. D: Appl. Phys.* **1998**, *31*, 2338−2353.

(18) Wu, J.; Ben, Y.; Chang, H.-C. Particle Detection by Micro-Electrical Impedance Spectroscopy with Asymmetric-Polarization AC Electroosmotic Trapping. *J. Microfluidics Nanofluidics*, in press.

(19) Wu, J.; Chang, H.-C. Asymmetrically Biased AC Electrochemical Micropump, *AIChE Annual Meeting 2004*, Nov. 7−12, Austin, TX.

(20) Lastochkin, D.; Zhou, R.; Wang, P.; Ben, Y.; Chang, H.-C. Electrokinetic micropump and micro-mixer design based on AC faradaic polarization. *J. App. Phys*. **2004**, *96*, 1730−1734.

Received for review July 2, 2004
Revised manuscript received January 8, 2005
Accepted January 11, 2005

IE049417U